EFFECT OF B_2O_3 ADDITION ON THE ELECTROCHEMICAL PERFORMANCE OF $LiVMoO_6$ CATHODE MATERIAL

Margarita Milanova, Reni Iordanova

Institute of General and Inorganic Chemistry, Bulgarian Academy of Sciences, G. Bonchev, str. bld. 11, 1113 Sofia, Bulgaria
E-mail: margi71@abv.bg

Received 07 May 2019
Accepted 31 July 2019

ABSTRACT

In this paper, we report for the preparation of $LiVMoO_6$ cathode material with and without B_2O_3 addition (B-LVM and LVM) by melt quenching method followed by heat treatment at 580°C. XRD, Raman and SEM investigations were performed to examine the phase formation, local structure and morphology of the obtained products. The results indicate that B_2O_3 acts as a sintering agent. The synthesized B-LVM material is comprised of clusters of agglomerated tightly packed small particles. The electrochemical performance of B-LVM and LVM as cathodes in lithium ion batteries was examined. The specific capacity estimated of the B_2O_3 – added $LiVMoO_6$ approaches 300 mAh g^{-1} which is larger than the specific capacity reported so far in the literature for this material. Although that the addition of the B_2O_3 enhances the capacity does not improve the cycling stability of the $LiVMoO_6$.

Keywords: boron oxide, $LiVMoO_6$, lithium batteries.

INTRODUCTION

It is generally believed that the capacity of the cathode materials is one of the major factors of the performance of Lithium-ion batteries (LIBs) [1, 2]. Recently a great number of vanadates containing transition metal ions, [3, 4] have been extensively studied as a possible electrode active materials in lithium batteries. Among them, the Brannerite-type $LiVMoO_6$ have attracted special attention both as cathode and anode material because of its open structure and interesting characteristic from a stand point of the variety of oxidation state [5 - 13]. Despite the high specific capacity (250 mAh g^{-1} between 1.5 and 3.5 V), $LiVMoO_6$ suffers from fundamental problems including low initial Coulombic efficiency and a long life cycling instability. A significant capacity fade during the cycles shows that irreversible structural and morphological changes take place in the electrode material upon lithium insertion [7, 8, 14].

There are several papers reporting that the introduction of a boron oxide to layered lithium transitional metal oxide leads to increase their conductivity and structural stability. [15 - 20]. This improvement is associated with the expansion of the interlayer distances with boron doping, leading to a much easier lithium ion intercalation/deintercalation [15, 20]. The strong B-O bonds can enhance the structural stability of the cathode [17, 19]. As a well-known sintering agent, the addition of B_2O_3 to the cathode will improve its density and structural integrity [16].

In the present work, we have investigated the effect of B_2O_3 addition on the structure and electrochemical performance of $LiVMoO_6$ cathode material.

EXPERIMENTAL

The homogenized batch of the Li_2CO_3; V_2O_5, MoO_3 and H_3BO_3 with appropriate composition for the $90LiVMoO_6.10B_2O_3$ molar ratio was melted in alumina crucible for 20 min at 800°C in air atmosphere. According to the electron microprobe analysis (EMRA), performed in our previous studies, the amount of Al_2O_3 dissolved into the glasses obtained by melting in alumina crucibles is at about 8 - 10 mol % [21]. Amorphous

sample was obtained by quenching of the melt between two stainless steel plates. The quenched sample was heat treated 5 h at 500°C and 10 h at 580°C in order to obtain well crystallized materials, denoted here as B-LVM. For the cake of comparison $LiVMoO_6$ denoted here as LVM without B addition was prepared, using the same procedure. The obtained materials were characterized by X-ray diffraction (XRD), differential thermal analysis (DTA), Raman spectroscopy, and scanning electron microscopy (SEM). X-ray diffraction measurements were conducted using CuK_a radiation in a laboratory X-ray diffractometer (Ultima IV, Rigaku Corp.). The thermal parameters of the B-LVM amorphous sample obtained were determined using differential thermal analysis (DTA) (Thermo Plus TG8110, Rigaku). Raman measurement of B-LVM and LVM were performed in the range 200 - 1200 cm^{-1} on a micro-Raman system from Jobin–Yvon Horiba (LABRAM HR-800) spectrometer with green laser (wavelength: 532 nm). The morphology and microstructure of B-LVM and LVM were investigated by scanning electron microscope (JEOL, JSM-5300).

Cycling performance of B-LVM and LVM was tested by construction of Li/B-LVM and Li/LVM cells employing liquid electrolyte. The composite cathode consisted of a mixture of active material (B-LVM and LVM, respectively) acetylene black and 8 wt % polyvinylidene fluoride (PVDF) dissolved in N-methylpyrrolidone (NMP) in 90:5:5 weight ratio. After mixing of the electrode materials, the slurries were painted on a stainless mesh (1 × 1 cm) as a current collector. Then, the electrodes were dried at 130°C for 3 h and pressed between stainless steel plates under 280 MPa. The prepared electrodes as a working electrodes and single lithium foil used as both the counter and reference electrode were put into the three-electrode - type electrochemical cells. The electrolyte used for analysis was 1M $LiPF_6$ dissolved in ethylene carbonate/diethyl carbonate (EC/DEC, 33/67). Cells were assembled in an argon-filled glove box. The prepared test cells were discharged and charged in the potential range from 1.8 to 3.7 V under a current density of 0.1 mA cm^{-2} at room temperature in Ar atmosphere using a charge-discharge measuring device (BTS-2004; Nagano). Electrochemical impedance measurements of the test cells before and after discharge - charge measurements were performed using a charge-discharge measuring device (SI1260 Solartron) in the frequency range from 100 to 1 MHz.

RESULTS AND DISCUSSION

Phase characterization and microstructure investigation

X-ray amorphous sample was obtained by quenching of the melt with composition $90LiVMoO_6.10B_2O_3$ (Fig. 1a). The as-quenched $90LiVMoO_6.10B_2O_3$ sample was investigated by differential thermal analysis (DTA) in order to establish the temperature at which the crys-

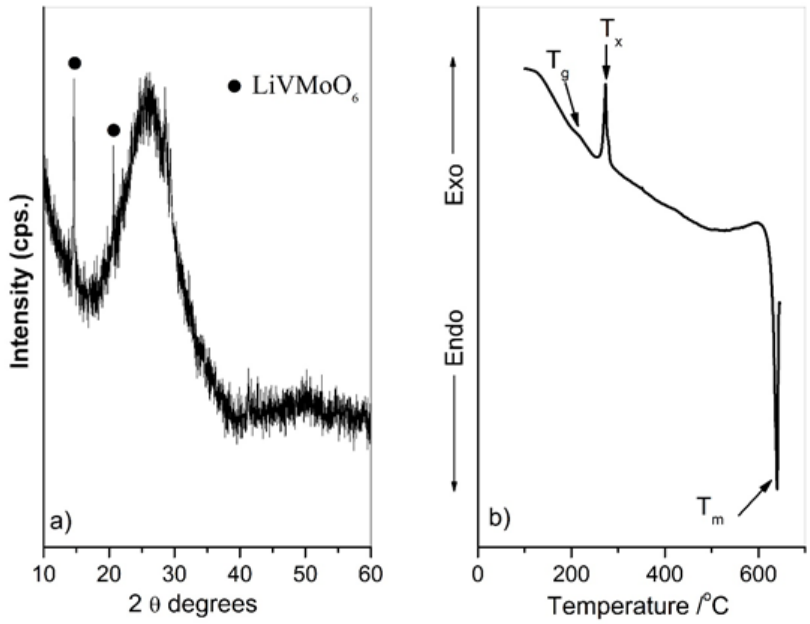

Fig. 1. XRD pattern (a) and DTA curve (b) of $90LiVMoO_6.10B_2O_3$ sample obtained by melt quenching.

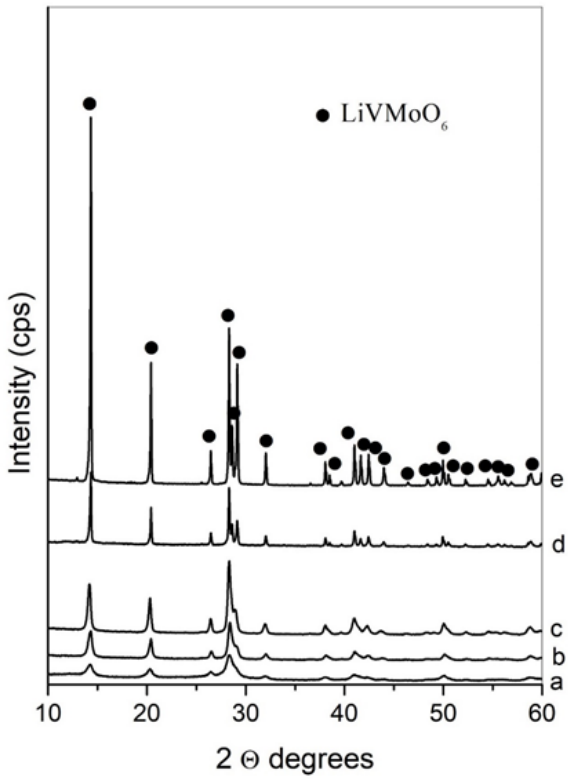

Fig. 2. XRD patterns of $90LiVMoO_6.10B_2O_3$ samples obtained by melt quenching and calcined at: a) 270°C for 5 hours; b) 450°C for 5 hours; c) 500°C for 5 hours; d) 500°C for 5 hours and at 580°C for 10 hours, and e) XRD pattern of pristine $LiVMoO_6$ obtained by melt quenching and calcined at 500°C for 5 hours and at 580 for 10 hours.

tallization of $LiVMoO_6$ starts. The DTA curve (Fig. 1b) contains a hump at 215°C corresponding to the glass transition temperature (T_g), followed by an exothermic peak at 270°C, due to the crystallization (T_x) of $LiVMoO_6$ and an endothermic effect at 640°C , attributed to the thermal decomposition (T_m) of $LiVMoO_6$ [8, 10, 12]. Having in mind DTA data obtained, the quenched $90LiVMoO_6.10B_2O_3$ sample was calcined for 5 hours at various temperatures in order to obtained well crystallized material (Fig. 2). As one can see the patterns obtained for the samples calcined for 5 hours at 270°C (Fig. 2a); 450°C (Fig. 2b) and 500°C (Fig. 2c), respectively show broad and poorly resolved diffraction peaks characteristic for the $LiVMoO_6$ phase. All the peaks are indexed assuming a C2/m symmetry that corresponds to the monoclinic citing of the brannerite structure [22]. The diffraction pattern of the B_2O_3-added $LiVMoO_6$ heat-treated for 5 h at 500°C and additionally for 10 h at 580°C (B-LVM) exhibits a well resolved peaks compared to those calcined at lower temperatures and for less time. Hence, despite that the crystallization starts around 270°C, well-crystallized $LiVMoO_6$ phase have been obtained at 580°C. Impurity peaks that could originate from the boron and lithium components were not observed in the XRD pattern. For the sake of comparison, pure $LiVMoO_6$ material was prepared in the same way (Fig. 2e). According to the XRD data, the diffraction lines in the XRD pattern of the boron added $LiVMoO_6$ (B-LVM) (Fig. 2d) are less intense as compared to the $LiVMoO_6$ without B_2O_3 (LVM) (Fig. 2e) which indicates poorer crystallinity and/or higher degree of aggregation of the particles. This suggestion is also confirmed by the Raman analysis. Fig. 3 compares Raman spectra of B-LVM and LMV obtained. Raman spectra of both samples contain the absorption bands typical for the various MeO_6 (Me = V, Mo, Li) octahedral units building the lattice [8, 23, 24]. Table 1 presents the detailed assignment of the Raman bands observed. As it is seen from the Fig. 3, Raman spectrum of the boron - added $LiVMoO_6$ (B-LVM) contains broader and less intense absorption bands than the bands in the spectrum of pristine $LiVMoO_6$ sample (LVM), evidencing its lower degree of crystallinity. As there is no noticeable shift in the bands position, it could be assumed that addition of the B_2O_3 does not influence the local structure of the $LiVMoO_6$. Probably no boron

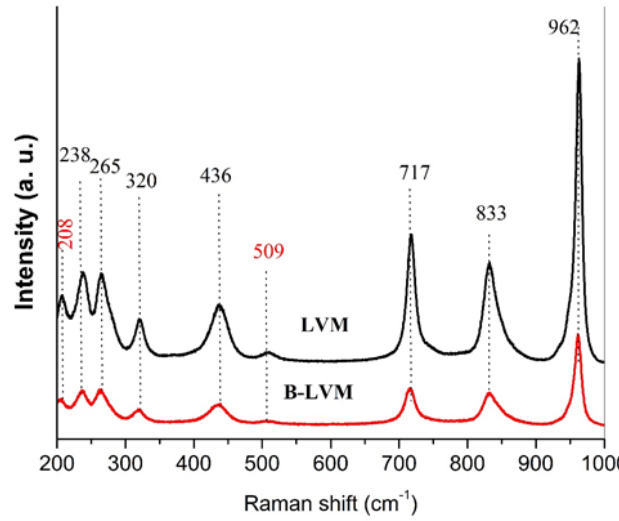

Fig. 3. Raman spectra of pristine $LiVMoO_6$ (LVM - black), and B_2O_3 - added $LVMoO_6$ (B-LVM - red) obtained by melt quenching and calcined for 5 hours at 500°C and for 10 hours at 580°C.

Table 1. Observed Raman bands and their assignment of B_2O_3 - added $LiVMoO_6$ (B-LVM) and pristine $LiVMoO_6$ (LVM) obtained.

Raman band positions (cm^{-1}) /Intensity	Assignments	Ref.
962/*vs*	ν (Me=O; Me=V, Mo)	8, 23, 24
833/*s*	ν_{as} (Me-O-Me)	8, 23, 24
717/*s*	ν_{as} (Me-O-Me)	8, 23, 24
509/w	ν (V_2O_2)	8
436/s	ν_s (Me-O-Me)	8, 23, 24
320/*w*	δ (Me-O-Me)	8, 23
265/*m*	δ (Me-O-Me)+ ν(LiO_6)	8, 23, 24
208/w	lattice modes	8

vs very strong; s strong; m medium; w weak

is incorporated within $LiVMoO_6$ during the synthesis and B_2O_3 has a sintering effect only. SEM investigations confirmed this suggestion. SEM images at different magnifications of $LiVMoO_6$ with and without B_2O_3 addition (B-LVM and LVM) obtained are shown on Fig. 4. a,b and c,d, respectively. As it is seen from the figure, B-LVM is characterized with a sintered microstructure and a higher degree of particles aggregation as compared with the pure $LiVMoO_6$. The SEM micrographs of the boron added $LiVMoO_6$ also show that the particles of B-LVM are smaller and have more irregular shape as compared with the particles of pure $LiVMoO_6$, which coincides well with the XRD data obtained.

Electrochemical characterization

The electrochemical charge/discharge measurements of B_2O_3-added $LiVMoO_6$ (B-LVM) and pristine $LiVMoO_6$ (LVM) obtained were carried out using Li

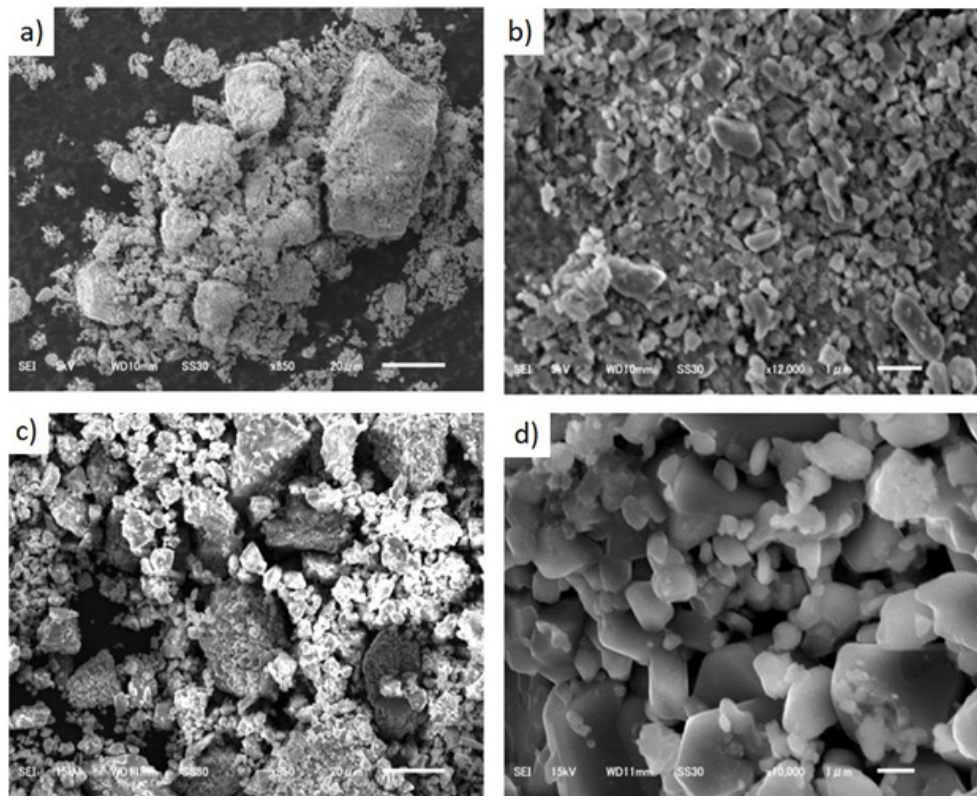

Fig. 4. SEM images of B_2O_3 - added $LVMoO_6$ (B-LVM) (a, b) and pristine $LiVMoO_6$ (LVM) (c, d) obtained by melt quenching technique and calcined for 5h at 500°C and 10 h at 580°C.

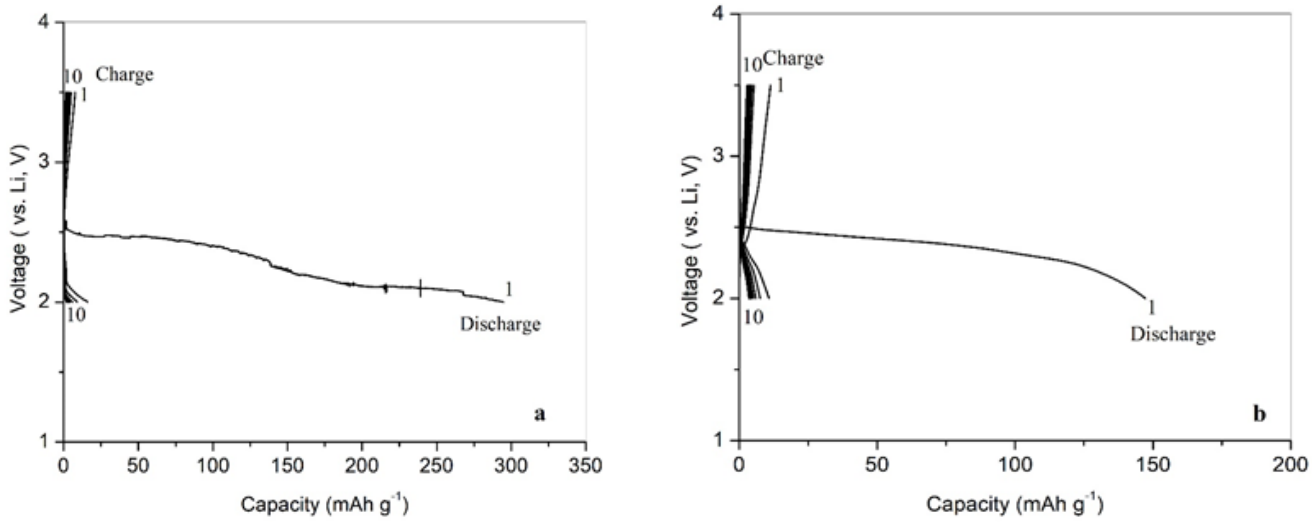

Fig. 5. Discharge-charge curves of Li/B-LVM (a) and Li/LVM (b) test cells cycled from 2.0 to 3.5 V.

metal as a counter electrode between 2.0 and 3.5 V under a current density of 0.05 mA cm^{-2} at 25°C. The discharge-charge curves of the test cells for 10 cycles are shown in Fig. 5. As it is seen from the figure, B-LVM shows significantly higher first discharge capacity approaching 300 mAh g^{-1}, as compared with the LVM, delivering a first discharge capacity at about 150 mAh g^{-1} when cycled from 2 to 3.5 V against Li metal. The specific capacity of boron-added $LiVMoO_6$ (B-LVM) estimated is larger than the specific capacity reported so far in the literature for this material (250 mAh g^{-1}) [8]. One possible reason for the enhanced capacity of B-LVM may be the smaller particles of boron-added $LiVMoO_6$. Since electrochemical lithium intercalation and deintercalation are generally limited by the rate of diffusion, the smaller grain size can favor the lithium-ion mobility in the particles by reducing the ion-diffusion pathway [12, 25]. However, the capacity drops sharply by more of 95 % after the first cycle, which indicates instability of the both crystalline phases investigated. The electrochemical data show that the addition of the B_2O_3 enhances the capacity but does not improve the cycling stability of the $LiVMoO_6$.

In order to understand the cycling behavior of the Li/B-LVM and Li/LVM cells, ac impedance measurements were carried out. Fig. 6 compares the impedance spectra of test cells before and after discharge-charge for 10 cycles. The impedance spectrum of both B-LVM and LVM electrodes are very similar in shape and contain three semicircles of different sizes. The high-frequency

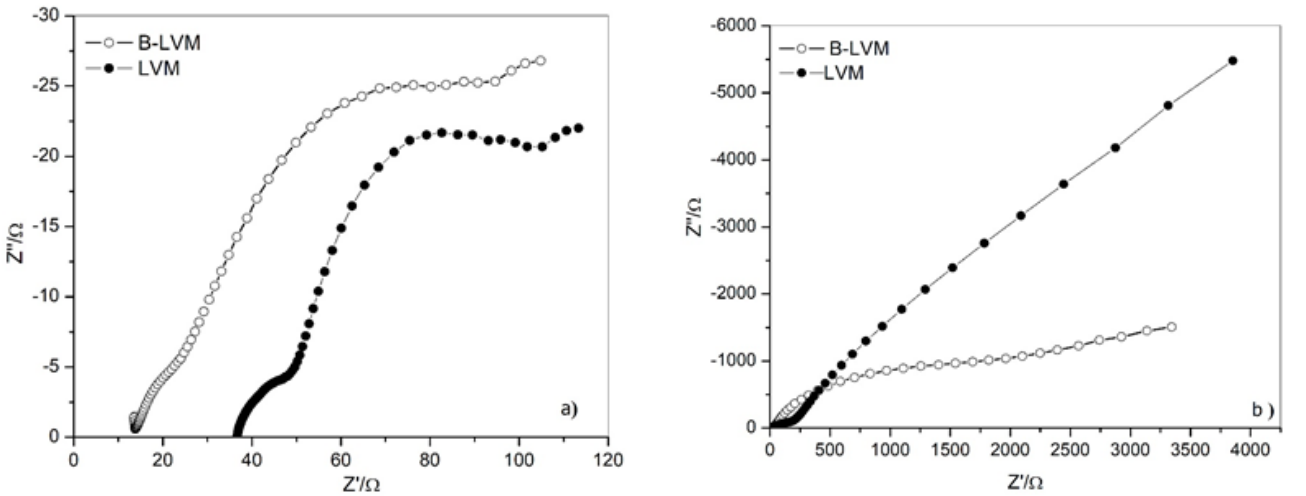

Fig. 6. Impedance spectra of Li/B-LVM and Li/LVM test cells before (a) and after (b) cycling.

smaller semicircle can be attributed to the resistance of the passive film on the cathode [17, 26, 27]. The formation of the passive film on the cathode is caused by the high potential between the cathode and the electrolyte interfaces at the fully charged stated. During cycling, this potential causes the electrolyte decomposition on the cathode [26]. The larger low frequency semicircle can be attributed to the charge transfer resistance across the interface between the liquid electrolyte and B-LVM and LVM, respectively [17, 27]. The third, smaller semicircle in the low frequency region can be assigned as the ionic diffusion of the electrolyte [28]. The ac impedance spectra of the both Li/B-LVM and Li/LVM tested cells are characterized with an incomplete semicircle with a large diameter corresponding to a capacitive behavior (blocking electrode effect) [22]. This result shows that obtained materials suffered from the structural instability leading to the sharp decreasing of the specific capacity. Further studies over the factors affecting the electrochemical behavior of B_2O_3-added $LiVMoO_6$ as positive electrode active material in lithium-ion batteries are needed.

CONCLUSIONS

Crystalline $LiVMoO_6$ with addition of 10 mol % B_2O_3 was synthesized by melt quenching method followed by heat treatment in order to increase the degree of crystallinity of the material. The obtained B_2O_3-added $LiVMoO_6$ (B-LVM) was compared by pristine $LiVMoO_6$ (LVM), prepared in the same way. It was found that the B_2O_3 added has a sintering effect only and does not change the layered structure of $LiVMoO_6$. The cycling discharge-charge behavior of the B-LVM as positive electrode in test cells employing liquid electrolyte evidenced that the addition of the B_2O_3 significantly enhances the specific capacity but does not improve the cycling stability of the $LiVMoO_6$.

Acknowledgements

The experiments were performed with equipment included in the National Infrastructure NI SEVE supported by the Ministry of Education and Science under grant agreement № DO1-160/28.08.18. Some of this work was done while the author M. Milanova was visiting the Department of Applied Chemistry, Graduate School of Engineering, Osaka Prefecture University under financial support by The Matsumae International Foundation (MIF) in the framework of the Matsumae International Fellowship Program April-September 2014.

REFERENCES

1. R. A. House, L. Jin, U. Maitra, K. Tsuruta, J. W. Somerville, D. P. Förstermann, F. Massel, L. Duda, M. R. Roberts and P. G.Bruce, Lithium manganese oxyfluoride as a new cathode material exhibiting oxygen redox, Energy Environ. Sci., 11, 2018, 926-932.
2. R. Yu, X. Wang, D. Wang, L. Ge, H. Shu, X. Yang, Self-assembly synthesis and electrochemical performance of $Li_{1.5}Mn_{0.75}Ni_{0.15}Co_{0.10}O_{2+\delta}$ microspheres with multilayer shells, J. Mater. Chem. A, 3, 2015, 3120-3129.
3. N.A. Chernova, M. Roppolo, A.C. Dillon, M.S. Whittingham, Layered vanadium and molubdenum oxides: batteries and electrochromics, J. Mater. Chem., 19, 2009, 2526-2552.
4. M.S. Whittingham, Lithium batteries and cathode materials, Chem Rev., 104, 2004, 4271-4301.
5. M. Michael, A. Fauzi, S.R.S. Prabaharan, Soft-combustion (wet chemical) synthesis of a new 4-V class cathode-active material, $LiVMoO_6$, for Li-ion batteries, Int. J. Inorg. Mater., 2, 2000, 261-267.
6. C. Julien, 4-Volt cathode materials for rechargeable lithium batteries wet chemistry synthesis, structure and electrochemistry, Ionics 6, 2000, 30-46.
7. R. Liu, C. Wang, L. Jang, J. Lee, A New Anode Material $LiVMoO_6$ for Use in Rechargeable Li-Ion Batteries, Tamkang J. Sci. Eng., 5, 2002, 107-112.
8. N. Amdouni, H. Zarrouk, F. Soulette, C. Julien, Synthesis, structure and lithium intercalation reaction in $LiVMoO_6$ brannerite-type materials, J. Mater. Sci., 13, 2003, 2374-2380.
9. R. Liu, Y. Wang, V. Drozd, S. Hu, H. Sheu, A Novel Anode Material $LiVMoO_6$ for Rechargeable Lithium-Ion Batteries, Electrochem. Solid State Lett., 8, 2005, A650-A653.
10. Y. Liang, S. Yang, Z. Yi, M. Li, J. Sun, Y. Zhou, Rheological phase synthesis and electrochemical performances of $LiVMoO_6$ as a high-capacity anode material for lithium ion batteries, J. Mater. Sci., 40, 2005, 5553-5555.
11. Y. Liang, X. Han, C. Cong, Z. Yi, L. Zhou, J. Sun, K. Zhang, Y. Zhou, Controlled synthesis of rod-like $LiVMoO_6$ nanocrystals for application in lithium-ion batteries, Nanotechnology, 18, 2007, 135607-135613.
12. L. Zhou, Y. Liang, L. Hu, X. Han, Z. Yi, J. Sun, S. Yang, Much improved capacity and cycling perfor-

mance of $LiVMoO_6$ cathode for lithium ion batteries, J. Alloys Comp., 457, 2008, 389-393.
13. N. Chen, C. Wang, F. Hu, X. Bie, Y. Wei, G. Chen, F. Du, Brannerite-type vanadium−molybdenum oxide $LiVMoO_6$ as a promising anode material for lithium-ion batteries with high capacity and rate capability, ACS Appl. Mater. Interfaces, 7, 2015, 16117-16123.
14. B.L. Cushing, S.H. Kang, J.B. Goodenough, Instability of brannerite cathode materials upon lithium insertion, Int. J. Inorg. Mater., 3, 2001, 875-879.
15. M. Vijayakumar, G. Hirankumar, M. S. Bhuvaneswari, S. Selvasekarapandian, Influece of B_2O_3 doping on the conductivity of $LiTiO_2$ electrode material, J. Power Sources, 117, 2003, 143-147.
16. S. Jouanneau, W. Bahmet, K.W. Eberman, L.J. Krause, J.R. Dah, Effect of Sintering Agent, B_2O_3,on $Li[Ni_xCo_{1-2x}Mn_x]O_2$ Materials, J. Electrochem. Soc., 151, A1789-A1796.
17. Z. Sun, X. Lingqun, D. Caigiao, Z. Hongtao, M. Zhang, L. Yiyang, Z. Ying, H. Yu, C. Yongsheng, Enhanced cycling stability of boron-doped lithium-rich layered oxide cathode materials by suppressing transition meal migration, J. Mater. Chem. A, 00, 2013, 1-9.
18. H.S. Jadhav, R.S. Kalubarme, S. Jang, K. Jung, K. Shin, C. Park, B_2O_3-added lithium aluminum germanium phosphate solid electrolyte for Li-O_2 rechargeable batteries, Dalton Trans., 43, 2014, 11723-11727.
19. S. Han, J. Song, T. Yim, Y. Kim, J. Yu, S. Yoon, Communication-Improvement of Starting Stability during High-Voltage Cycling in High-Nickel Cathode Materials with B_2O_3 Addition. J. Electrochem. Soc., 163, 2016, A748-A750.
20. Y.Feng, Y. Li, F. Hou, Boron doped lithium trivanadate as a cathode material for an enhanced rechargeable lithium ion batteries, J. Power Sources, 187, 2009, 224-228.
21. R. Iordanova, M. Milanova, L. Aleksandrov, A. Staneva, Y. Dimitriev, Glass formation and structure of glasses in the WO_3-ZnO-Nd_2O_3-Al_2O_3 system, J. Non-Cryst. Solids, 414, 2015, 42-50.
22. R. Run, A. Wadsley, The crystal structure of $ThTi_2O_6$ (brannerite), Acta Cryst., 21, 1966, 974-978.
23. M. Milanova, R. Iordanova, M. Tatsumisago, A. Hayashi, P. Tzvetkov, D. Nihtianova, P. Markov, Y. Dimitriev, Soft mechanochemical synthesis and electrochemical behavior of $LiVMoO_6$ for all-solid-state lithium batteries, J Mater Sci., 51, 2016 3574-3584.
24. E. J. Baran, C. I. Cabello, A. G. Nord, Raman spectra of some $M^{II}V_2O_6$ brannerite- type metavanadates, J Raman Spectrosc., 18, 1987, 405-407.
25. N. Amdouni, H. Zarrouk, C.M. Julien, Synthesis, structure and intercalation of brannerite $LiVWO_6$ wet-chemical products, J. Mater. Sci., 38, 2003, 4573-4579.
26. J. Li, E. Murphy, J. Winnick, P.A. Kohl, Stidies on the cycle life of commercial lithium ion batteries during rapid charge-discharge cycling, J. Power Sources, 102, 2001, 294-301.
27. S. Rodrigues, N. Munichandraiah, A.K.Shikula, AC impedance and state-of-charge analysis of a sealed lithium-ion rechargeable battery, J. Solid State Electrochem., 3, 1999, 397-405.
28. T. Apriani, W.S. Arsyad, P. Wulandari, R. Hidayat, Investigation on the influence of layer structure and nano porosity of light scattering TiO_2 layer in DSSC, Journal of Physics: Conference Series, 739, 2016, 012134.